Accurate statistical extraction of AlGaN/GaN HEMT device parameters using the Y-function

R. Kom Kammeugne, C. Leroux, J. Cluzel, L. Vauche, C. Le Royer, A. Krakovinsky, R. Gwoziecki, J. Biscarrat, F. Gaillard, M. Charles, et al.

Version of Record: https://www.sciencedirect.com/science/article/pii/S0038110121001234
Manuscript_cda45f3fd08a26df272d6ba2456c0aba

Accurate Statistical Extraction of AlGaN/GaN HEMT Device Parameters Using the Y-function

R. Kom Kammeugne[a⋆], C. Leroux[a], J. Cluzel[a], L. Vauche[a], C. Le Royer[a], A. Krakovinsky[a], R. Gwoziecki[a], J. Biscarrat[a], F. Gaillard[a], M. Charles[a], E. Bano[c] and G. Ghibaudo[c]

[a] Univ. Grenoble Alpes, CEA, Leti, F-38000, Grenoble, France

[c] Univ. Grenoble Alpes, IMEP-LAHC, MINATEC/INPG, 3 Parvis Louis Néel, 38016 Grenoble, France

E-mail address: romeo.komkammeugne@cea.fr

***Abstract*—A new protocol based on Y-function is used for accurate statistical extraction of electrical parameters of High Electron Mobility Transistor (HEMT) devices for GaN technology. This protocol presented here is used for extraction of relevant electrical parameters such as oxide capacitance, threshold voltage, effective mobilities and access resistance. This study has been verified over a large range of channel lengths for two normally-off HEMT GaN wafers having different levels of access resistances.**

***Keywords*—Statistical electrical characterization, Y-function, Normally-off, High-Electron-Mobility-Transistor (HEMT), Gallium Nitride (GaN); Electron mobility, 2DEG.**

I. INTRODUCTION

Gallium Nitride (GaN)-based high-electron mobility transistors (HEMTs) have attracted a lot of attention in power electronics and RF applications which require high breakdown voltage and low ON-resistance [1]–[3]. However, the extraction of electrical parameters is a key point to understand the physical phenomena that govern the operation of power transistors mainly for short channel devices.

Recently, the process influence on two-dimensional electron gas (2DEG) transport properties in $Al_{0.25}Ga_{0.75}N$/AlN/GaN heterostructures has been discussed extensively on various technological splits (normally on & off) [1], [2]. Since for GaN-based HEMT devices, the ON-state resistance is a critical issue [4], a relevant extraction methodology should include the impact of access resistance. For Si device technology, a specific methodology has been proposed [5]–[11] using a Y-function based I_d-V_g characteristic.

The Y-function eliminates the influence of bias-independent source-drain series resistance [5] and we presented on a previous work [12] its first use for GaN HEMT devices.

The aim of this study is to extract threshold voltage (V_{th}) and effective mobility (μ_{eff}) independently of access resistance (R_{SD}). We will first describe the experiment performed in this study: process technology, studied wafers and electrical characterization. We will then introduce the Y-function method and its interest for parameter extraction. We will use it to extract various parameters, comparing them on

different wafers, and discriminating the respective impact of parasitic access resistance effects and process influence on material electrical parameters in GaN based HEMT devices.

II. Experiments

Electrical measurements were performed on two different wafers, processed with normally-off HEMT technology, having different levels of access resistance. GaN epitaxy (see Fig. 1) is performed by Metal-Organic Chemical Vapor Deposition (MOCVD), on a 200 mm diameter silicon (111) substrate. Starting with an AlN nucleation layer followed by AlGaN and unintentionally doped (UID) GaN buffer layer, an AlN spacer and an $Al_xGa_{1-x}N$ barrier layer are then grown on top, followed by in-situ deposition passivation layer [13], [14]. In this study, fully recessed MIS gate normally-off GaN transistors are processed by dry etching the AlGaN and UID-GaN layers at the gate.

Wafer 1 and 2 correspond to two different recess depths, RD1 and RD2 (RD1 > RD2) respectively, followed by the deposition of an oxide layer of Al_2O_3 by Atomic Layer Deposition and the metallic gate. The source and drain are composed of metallic Ohmic contacts (Ti/AlCu) connected to the 2DEG. The tested devices were 100 µm wide (W) with channel length (L_g) ranging from 0.5 µm to 50 µm. I_d-V_g characteristics have been measured on a B1500 Semiconductor Device Analyzer with gate bias from -1 to +5 V (V_d = 10 mV). C_{gc}-V_g capacitance characteristics were measured with the same gate bias range on an HP4284 LCR meter.

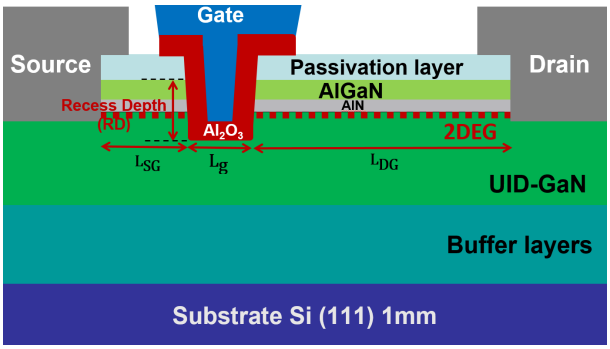

Fig. 1. Schematic cross section of Al_2O_3/GaN MIS-HEMT stack.

III. Experimental Extraction Methodology

Gate oxide capacitance (C_{ox}), V_{th} and μ_{eff} were first extracted using classical methodologies. We report in Fig.2, C_{ox} measurements at maximum V_g, showing an increase at shorter lengths. This may be due to an effective length L_{eff} larger than designed L_g, with an influence of recess depth. Using both C_{gc}-V_g and I_d-V_g characteristics in the linear regime (low V_d), split-CV mobility [6] (1) has been extracted versus channel carrier concentration N_{Ch} (Fig.3).

$$\mu_{split}(N_{ch}) = \frac{L_g}{W}\frac{I_d(V_g)}{Q_{Ch}(V_g)V_d} \quad (1)$$

where, $Q_{Ch}(V_g) = q.N_{ch}(V_g)$ is the total charge in the accumulation channel obtained from integration of C_{gc}-V_g characteristics.

Whereas $C_{ox}\left[C_{gc}(V_g=5V)/(W\cdot L_g)\right]$ values are quite similar for the two wafers, mobility dependence with L_g appears different, with a significant reduction for small L_g, especially for wafer 2. In order to investigate the origin of the reduction of μ_{split} with L_g, the Y-function method has been applied.

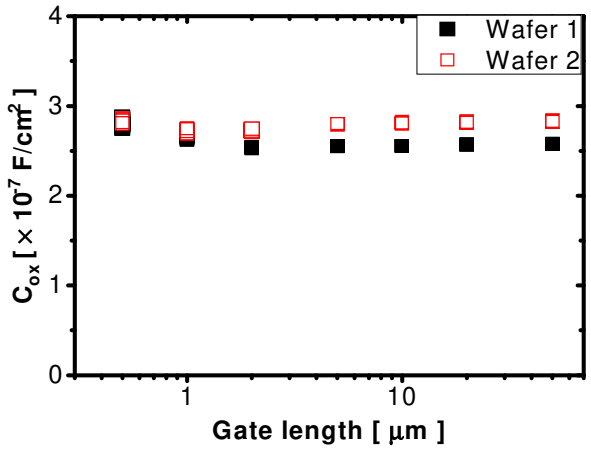

Fig. 2. Capacitance at V_g =5V for different L_g on wafer 1 and 2.

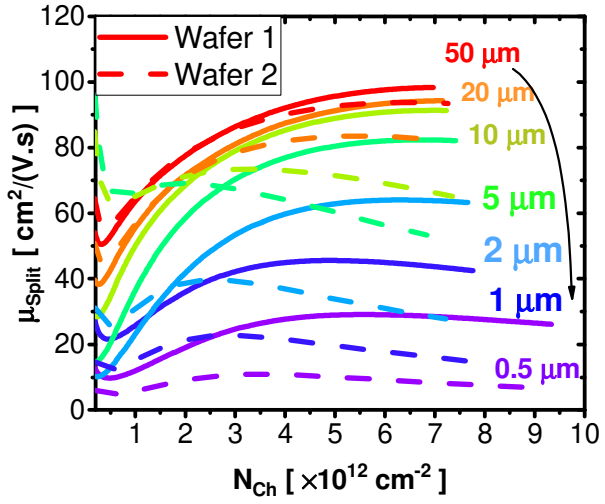

Fig. 3. Split-CV mobility versus N_{Ch} for different L_g on wafer 1 (solid line) and wafer 2 (dashed line).

The Y-function (2) is based on the I_d-V_g characteristic and its transconductance g_m, $g_m=\frac{dI_d}{dV_g}$ [5].

$$Y(V_g)=\frac{I_d(V_g)}{g_m^{1/2}} \quad (2)$$

It was demonstrated analytically that in accumulation regime, Y-function (2) must follow a linear trend $Y(V_g)=\sqrt{\beta \cdot V_d}\cdot(V_g-V_{th,Y})$ [5] for wich β is the trans-conductance parameter $(\beta = WC_{ox}\mu_0/L_g)$.

Experimentally, two GaN-HEMT devices (A and B) having different access resistances were selected on wafer 2. Fig.4 confirms the theoretical independence of Y-function with access resistance whereas I_d-V_g is significantly impacted. Y-function can be then used to extract HEMT parameters without any influence of the access resistance.

Indeed, Y-function (2) provides an easy and reliable way to extract, from its linear, a threshold voltage V_{th} value and a slope $\sqrt{\beta \cdot V_d}=(WC_{ox}\mu_0 V_d/L_g)^{1/2}$ that is the gain factor on MOSFET devices free from series resistance [5]. A low field mobility μ_0 can be extracted from the trans-conductance parameter β.

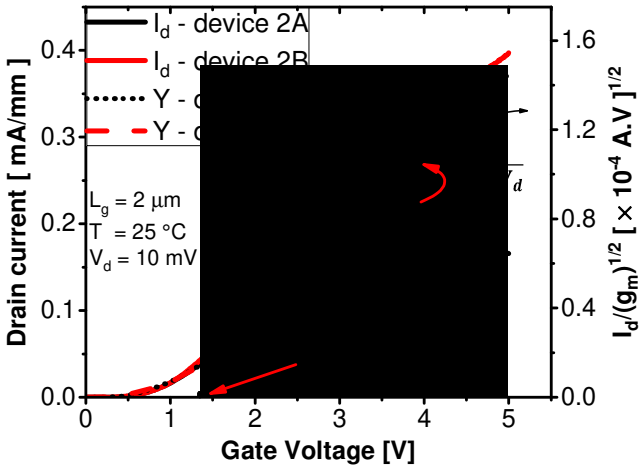

Fig. 4. Drain current and Y-function on the MIS-HEMT GaN technology for two devices (black line 2A and red line 2B) on wafer 2 having different access resistances.

Using Y, β and I_d, an additional θ_{eff} function (3) can be calculated for each device in order to extract the mobility attenuation factor θ_{eff}.

$$\theta_{eff}(V_g) = \frac{\beta . V_d}{I_d(V_g)} - \frac{\sqrt{\beta . V_d}}{Y(V_g)} \quad (3)$$

As already demonstrated [5], when the gate voltage increases, θ_{eff} saturates towards a value θ_1 called mobility reduction factor. As we compare GaN HEMTs with different L_g and thus different β, θ_1 is expected to follow a linear trend versus β such as ($\theta_1 = \theta_0 + R_{SD} \cdot \beta$ [5]) from which the source/drain access resistance R_{SD} can be extracted. Fig.5

shows the θ_{eff} function dependence with V_g for the two GaN HEMT devices reported in Fig. 4. This figure confirms the asymptotic behaviour of the $\theta_{eff}(V_g)$ functions, leading to the $\theta_{1,A}$ and $\theta_{1,B}$ values. It also confirms the dependence of θ_1 with R_{sd}, as $\theta_{1,A}$ is greater than $\theta_{1,B}$.

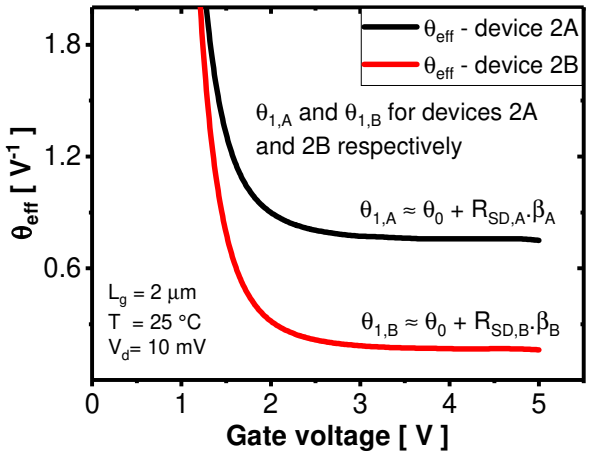

Fig. 5. θ_{eff}-function on the MIS-HEMT GaN technology on wafer 2 for two devices (black solid line 2A and red solid line 2B) having

For statistical parameters extraction, a mapping measurement of $C_{gc}(V_g)$ characteristics on all devices is time-consuming. For this reason, full $C_{gc}(V_g)$ characteristics were obtained only on a reference device and for different gate lengths.

Then, knowing $C_{gc}(V_g)$ reference characteristics, we calculate the channel charge of the reference device $Q_{Ch,Ref}(V_g)$. Next, measuring C_{gc} at $V_g = 5\,V$ for each device, we can deduce the channel charge $Q_{Ch,i}$ (4) as we know the oxide capacitance variability compared to reference device, and the threshold voltage dispersion ($\Delta V_{th,i} = V_{th,Ref} - V_{th,i}$) which is obtained by a mapping of drain current $I_d(V_g)$ measurement. The channel charge Q_{Ch} is then reconstructed for device i.

$$Q_{Ch,i} = \frac{C_{ox,i}}{C_{ox,Ref}} \cdot Q_{Ch,Ref}(V_g + \Delta V_{th,i}) \qquad (4)$$

where $C_{ox,i}$ $\left[C_{gc,i}(V_g=5V)/(W \cdot L_g)\right]$ is the oxide capacitance for the device i.

IV. Results and Discussion

A. Experimental results in MIS-HEMT GaN using the Y-function

Fig. 6 compares the median values of threshold voltages related to different definitions. $V_{th,lin}$ at low constant current ($I_d \cdot W/L_g$ with I_d=1nA) appears as the most stable parameter as we vary L_g, however it is below the effective onset of current. $V_{th,gm}$ extrapolated from I_d slope at maximum transconductance and $V_{th,Y}$ extrapolated from Y-function follow similar trends with a small gate length dependence. They both qualify the threshold of HEMT device but $V_{th,Y}$ is obtained from strong inversion regime and without any impact of series resistance. On the contrary, $V_{th,lin}$ at 10^{-5} A.mm^{-1} evidences a non-expected linear trend with increasing gate lengths likely due to an extraction in medium inversion especially for large L_g. It therefore cannot be considered as reliable indicator of HEMT threshold voltage.

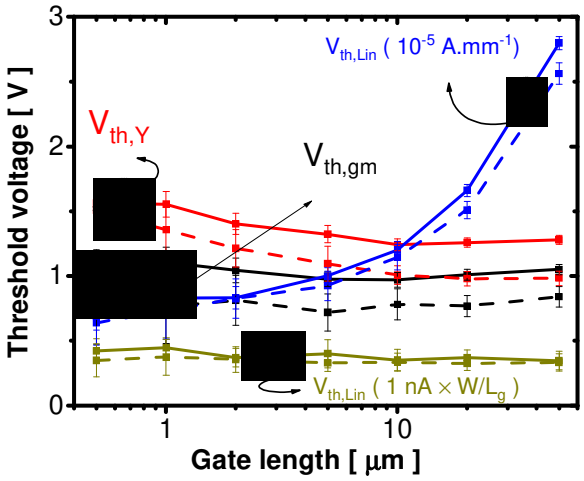

Fig. 6. Various median threshold voltages versus L_g on wafer 1 (solid line) and wafer 2 (dashed line).

Fig. 7 reports the dependence of θ_1 (median, standard deviation) for all tested devices versus gain factor β. A θ_0 value is obtained from the y-axis intercept at zero gain, providing $\theta_0 \approx 0.038$ V^{-1} for wafer 1 and $\theta_0 \approx 0.018$ V^{-1} for wafer 2. θ_0 can be considered as an intrinsic parameter of each processed wafer. Using a logarithmic scale (Fig.8), with θ_1 variation we see larger scattering of the source/drain access resistance (R_{SD}) value on wafer 2 (≈×10 compared to ≈×1.4 for wafer 1).

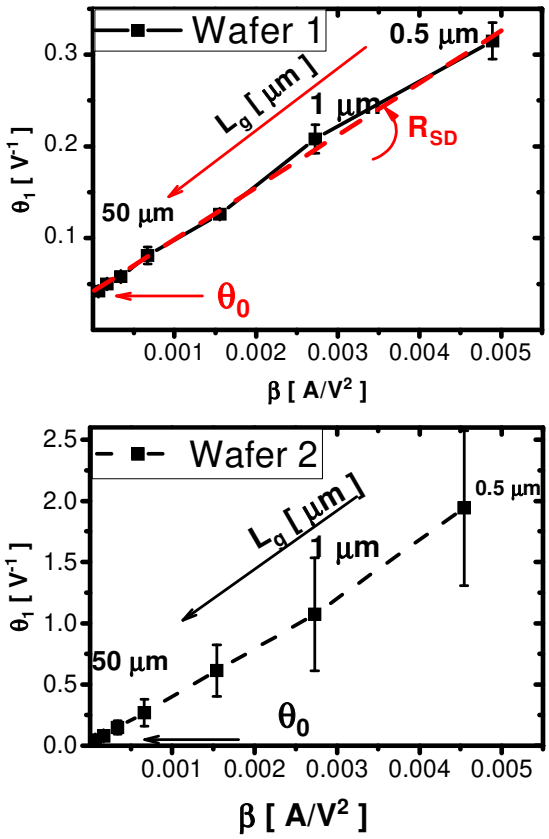

Fig. 7. Dependence of θ_1 function with β (median) for different L_g obtained from Y-function for wafer 1 ($\theta_0 \approx 0.0382$ V^{-1}) and wafer 2 ($\theta_0 \approx 0.018$V^{-1}).

For each device, we can estimate R_{SD} using θ_0, θ_1 and β (Fig. 9). Note that the estimation is more reliable for small gate lengths for which the hypothesis on the intrinsic mobility reduction factor θ_0 is less important. On wafer 1, R_{SD} is controlled at a moderate value of around 60 Ω whereas R_{SD} median value can reach up to 400 Ω for wafer 2 due to degraded Ohmic contact process.

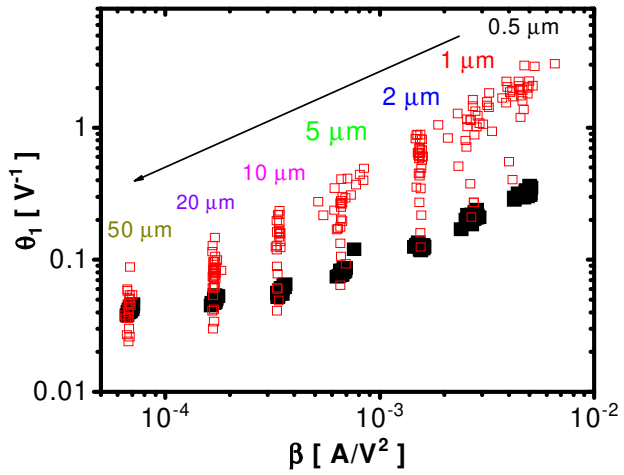

Fig. 8. Full report of θ_1 versus β in logarithmic scale for wafer 1 (full square) and wafer 2 (empty square).

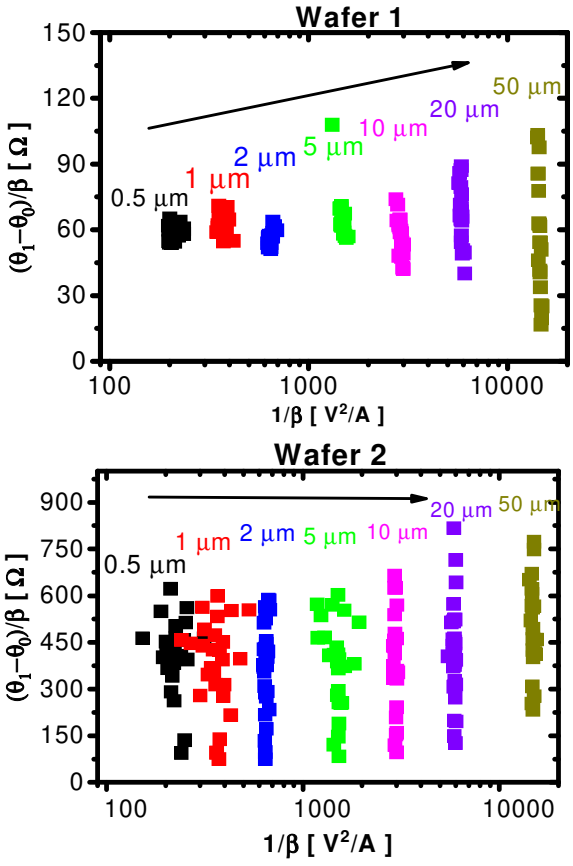

Fig. 9. Full report of plots of $\frac{\theta_1-\theta_0}{\beta}$ corresponding to the source/drain access resistance R_{SD} value, plotted here for each device on wafer 1 and wafer 2.

Using R_{SD} value extracted for each device, the split-CV mobility (μ_{split}) can be corrected according to the following equation:

$$\mu_{split\_corrected}=\mu_{split}\cdot\frac{V_d}{V_d-R_{SD}\cdot I_d} \quad (5)$$

where, μ_{split} (1) is the effective mobility obtained by classical split-CV method [6]. R_{SD} is the global access resistance of the HEMT device, it is obtained from θ_1 the asymptotic value of θ_{eff}, and it corresponds to the source and drain access resistance. R_{SD} value can be also estimated with the contact resistance (R_C) at source and drain, and the 2D gas resistance R_{2DEG} leading: $2R_C+R_{2DEG}\cdot(L_{SG}+L_{DG})/W$ (L_{SG} and L_{DG} the source-to-gate and drain-to-gate length respectively).

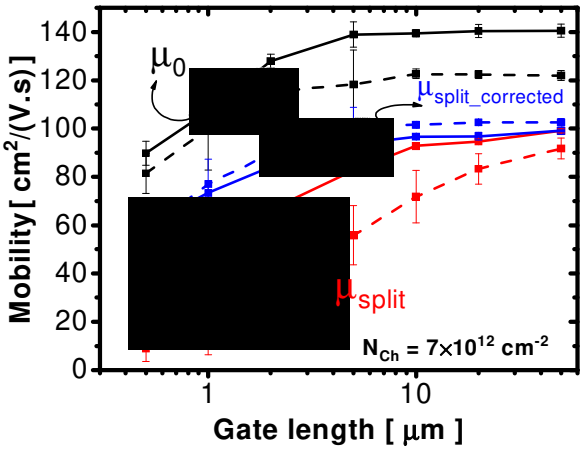

Fig. 10. Comparison of μ_0, μ_{split}, $\mu_{split\_corrected}$ versus gate length for wafer 1 (solid line) and wafer 2 (dash line).

In Fig. 10, we compare three mobility parameters: μ_0 obtained from β parameter, μ_{split} and $\mu_{split\_corrected}$ extracted for $N_{Ch}= 7\times10^{12}$ cm^{-2}.

Note that, the classical μ_{split} underestimates effective mobility, mainly for small L_g, due to parasitic bias drop in access resistances. As expected from literature [6], μ_0 slightly overestimates mobility, but it provides the same trend as $\mu_{split\_corrected}$ versus gate length. $\mu_{split\_corrected}$ can be considered as the best estimation of the HEMT mobility. The mobility measured at the Oxide/semiconductor interface is significantly degraded compared to the 2DEG mobility usually seen with an undamaged AlGaN/GaN interface [1], [2] [15].

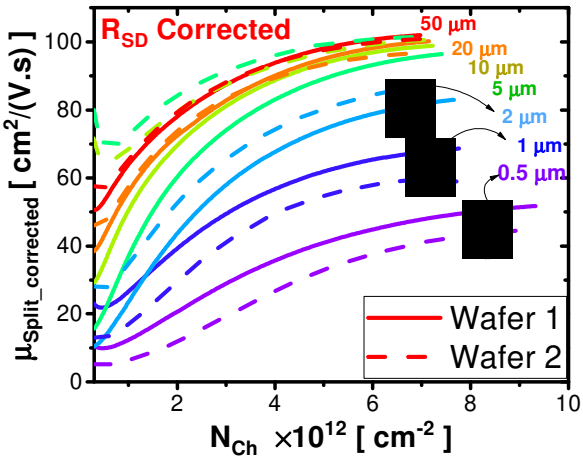

Fig. 11. Split-CV mobility corrected from R_{SD} effect versus N_{Ch} for different gate lengths for wafer 1 (solid line) and wafer 2 (dashed line).

Fig. 11 reports $\mu_{split\_corrected}$ for the same devices that are reported in Fig.3, but using the R_{SD} correction obtained for each device. Dependences for wafers 1 and 2 appear now similar with a similar decrease with gate lengths. The strong decrease of mobility seen on μ_{split} for wafer 2 (Fig.3) can be explained by the large value of R_{SD}. Using Y-function, even in the case of large access resistance, it is possible to extract the mobility in HEMT channel for short lengths for which the impact of access resistance is the strongest.

Fig.12 shows $I_d(V_g)$ characteristics of raw data (a). When we apply the correction process (Eq.5) using R_{SD} obtained by Y-function (1), we obtain the $I_d(V_g)$ characteristics with R_{SD} correction (Fig12(b)) for the same devices comparing these two figures, we can note the elimination of the parasitic

effect due to the bias drop in the access region. Wafer 2 was obtained with a preliminary process having non optimized Ohmic contact.

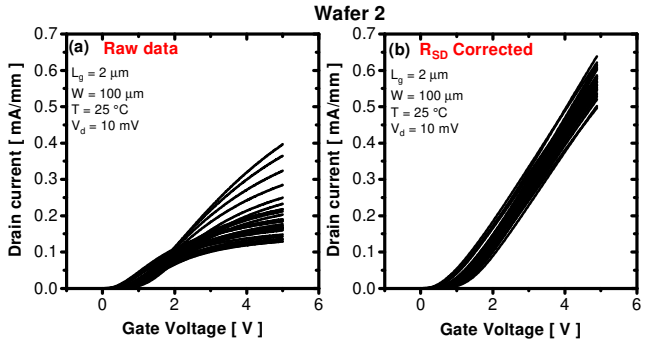

Fig. 12. $I_d(V_g)$ characteristics raw (a) and corrected (b) data in linear scale on the MIS-HEMT GaN technology for wafer 2.

B. Y-function dependence with channel charge and capacitance

In this section, we propose using the Y-function from depletion to accumulation for different gate lengths using the parameters extracted experimentally such as $\theta_1=\theta_0+R_{SD}\cdot\beta$ and slope $\sqrt{\beta\cdot V_d}$. This was performed on the MOS-HEMT GaN devices of wafer 2 for which the parameters are more degraded.

A new Y-function based extraction methodology applicable from weak to strong inversion and not limited to above or near threshold region has been developed for MOSFET parameter extraction under low voltage operation [8]. By analogy to the Y-function (Eq. 2) built from the drain current and transconductance, Henry et al. [8] proposed a Y-function build from accumulation charge and capacitance (Eq. 6). In strong accumulation, Y_c follows a linear trend.

$$Y_c = \frac{Q_{Ch}}{\sqrt{C_{gc}}} = \sqrt{C_{ox}}\cdot\left(V_g - V_{th}\right) \tag{6}$$

Assuming an exponential variation of Q_{Ch} in depletion, $(Q_{Ch} \approx Q_{Ch0}\, exp\left[\left(V_g - V_{th}\right)/nU_T\right])$ with $U_T = kT/q$ being the thermal voltage.

$C_{gc} \approx Q_{Ch}/nU_T$, yields for Y_c [8],

$$Y_c \approx \sqrt{nU_T Q_{Ch}} \tag{7}$$

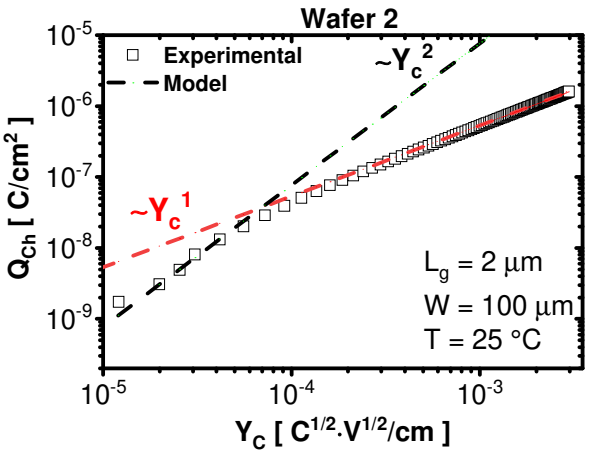

Fig. 13. Experimental variations (symbols) of Q_{Ch} with Y_c showing the asymptotic limits from weak to strong accumulation varying respectively as Y_c^2 and Y_c^1 (dashed lines).

In Fig. 13, the two asymptotic trends (Eqs. 6 & 7) are clearly identified on a $Q_{Ch}(Y_c)$ plot.

As a result, combining both asymptotic laws, a general expression of $Q_{Ch}(Y_c)$ valid from weak to strong accumulation can be proposed [8].

$$Q_{Ch} = C_{ox}\frac{\left(\frac{Y}{\sqrt{\beta V_d}}\right)^2}{\left(nU_T + \frac{Y}{\sqrt{\beta V_d}}\right)} \tag{8}$$

Considering the classical model for the drain current in linear operation:

$$I_d = \frac{W}{L}\cdot\mu_{eff}(V_g)\cdot Q_{Ch}(V_g)\cdot V_d \tag{9}$$

where μ_{eff} is the effective mobility, Q_{Ch} the channel charge and V_d the drain voltage.

Assuming μ_{eff} to be constant with $V_g(=\mu_0)$ in depletion and considering a single mobility degradation factor θ_1, the mobility in accumulation, μ_{eff} can be expressed using the conventional formulation (10) [5].

$$\mu_{eff}(\mathrm{V_g}) = \frac{\mu_0}{1+\theta_1\left(\frac{Q_{Ch}(V_g)}{C_{ox}}\right)} \qquad (10)$$

From Equations. 8, 9 and 10 we get:

$$\frac{Y^2}{I_d} = \frac{I_d}{g_m} = nU_T + \frac{Y}{\sqrt{\beta \cdot V_d}}\left[1 + \theta_1 \frac{Y}{\sqrt{\beta \cdot V_d}}\right] \qquad (11)$$

Equation (11) indicates that the variation of Y^2/I_d $(= I_d/g_m)$ with $\mathrm{Y(V_g)}$ should follow a parabolic behavior with coefficients providing the three parameters n, β and θ_1 [8].

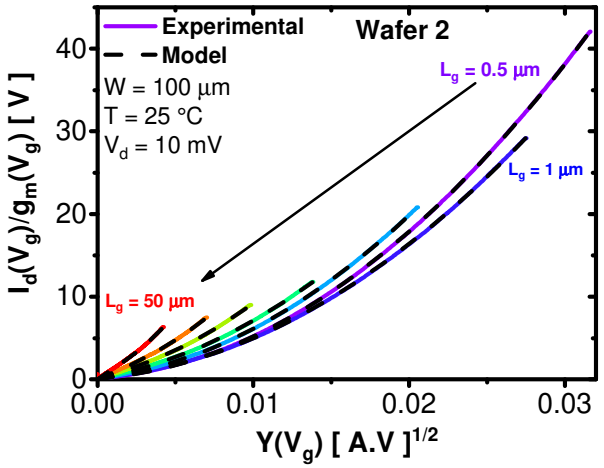

Fig. 14. Experimental (solid-lines) and modeled (dashed lines) I_d/g_m Characteristics for various gate lengths on the MIS-HEMT GaN technology for wafer 2.

Fig. 14 summarizes experimental values and model for different gate lengths. To fit the parabolic dependence, we get a set of θ_1 and β parameters for each gate length. We can see the good fit obtained for all gate lengths. Moreover θ_1 and β obtained by this method are similar to values obtained using respectively θ_{eff} asymptot (Eq.3) and $Y(V_g)$ slope (Fig.15).

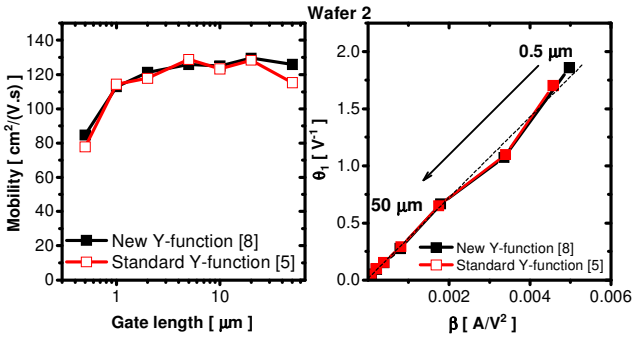

Fig. 15. Variation of μ_0 with gate length and θ_1 with β obtained from new Y-function and from standard Y-function on the MIS-HEMT GaN devices.

This extraction procedure proposed by [8] can be used for a systematics HEMTs parameter extraction applying for example a Levenverg-Marquardt non-linear regression to the Y^2/I_d versus $\mathrm{Y(V_g)}$ plots.

V. Conclusion

A statistical and accurate analysis of $\mathrm{I_d}$-$\mathrm{V_g}$ has been performed and the Y-function method was applied in GaN HEMT devices. It enables a reliable parameter extraction free from access resistance parasitic effects. Consequently, it allows a reliable extraction of intrinsic MOS parameters (i.e. $\mathrm{C_{ox}}$, $\mathrm{V_{th}}$ and mobility) on GaN HEMT devices, enabling statistical analysis of process variations on GaN HEMT device technology.

Acknowledgment

This work was supported by the French national program "programme d'investissements d'avenir IRTNanoelect" ANR-10-AIRT-05.

References

[1] I. Nifa *et al.*, 'Characterization and modeling of 2DEG mobility in AlGaN/AlN/GaN MIS-HEMT', *Microelectron. Eng.*, vol. 215, p. 110976, Jul. 2019, doi: 10.1016/j.mee.2019.05.003.

[2] C. Mizue, Y. Hori, M. Miczek, and T. Hashizume, 'Capacitance–Voltage Characteristics of Al $_2$ O $_3$ /AlGaN/GaN Structures and State Density Distribution at Al $_2$ O $_3$ /AlGaN Interface', *Jpn. J. Appl. Phys.*, vol. 50, no. 2, p. 021001, Feb. 2011, doi: 10.1143/JJAP.50.021001.

[3] Y. Zhao *et al.*, 'Effects of recess depths on performance of AlGaN/GaN power MIS-HEMTs on the Si substrates and threshold voltage model of different recess depths for the using HfO2 gate insulator', *Solid-State Electron.*, vol. 163, p. 107649, Jan. 2020, doi: 10.1016/j.sse.2019.107649.

[4] N. Zhang *et al.*, 'Large area GaN HEMT power devices for power electronic applications: switching and temperature characteristics', in *IEEE 34th Annual Conference on Power Electronics Specialist, 2003. PESC'03.*, 2003, vol. 1, pp. 233–237.

[5] G. Ghibaudo, 'New method for the extraction of MOSFET parameters', *Electron. Lett.*, vol. 24, no. 9, pp. 543–545, 1988.

[6] K. Romanjek, F. Andrieu, T. Ernst, and G. Ghibaudo, 'Improved Split C–V Method for Effective Mobility Extraction in sub-0.1-<tex>$muhbox m$</tex>Si MOSFETs', *IEEE Electron Device Lett.*, vol. 25, no. 8, pp. 583–585, Aug. 2004, doi: 10.1109/LED.2004.832786.

[7] T. A. Karatsori *et al.*, 'Full gate voltage range Lambert-function based methodology for FDSOI MOSFET parameter extraction', *Solid-State Electron.*, vol. 111, pp. 123–128, Sep. 2015, doi: 10.1016/j.sse.2015.06.002.

[8] J. B. Henry, Q. Rafhay, A. Cros, and G. Ghibaudo, 'New Y -function based MOSFET parameter extraction method from weak to strong inversion range', *Solid-State Electron.*, vol. 123, pp. 84–88, Sep. 2016, doi: 10.1016/j.sse.2016.06.004.

[9] A. Aminbeidokhti *et al.*, 'A method for extraction of electron mobility in power HEMTs', *Superlattices Microstruct.*, vol. 85, pp. 543–550, Sep. 2015, doi: 10.1016/j.spmi.2015.05.036.

[10] Y. Taur *et al.*, 'A new'shift and ratio'method for MOSFET channel-length extraction', *IEEE Electron Device Lett.*, vol. 13, no. 5, pp. 267–269, 1992.

[11] A. Ortiz-Conde, F. J. García-Sánchez, J. Muci, A. Terán Barrios, J. J. Liou, and C.-S. Ho, 'Revisiting MOSFET threshold voltage extraction methods', *Microelectron. Reliab.*, vol. 53, no. 1, pp. 90–104, Jan. 2013, doi: 10.1016/j.microrel.2012.09.015.

[12] R. K. Kammeugne *et al.*, 'Y-Function Based Methodology for Accurate Statistical Extraction of HEMT Device Parameters for GaN Technology', in *2020 Joint International EUROSOI (EUROSOI-ULIS)*, Caen, France, Sep. 2020, pp. 1–4, doi: 10.1109/EUROSOI-ULIS49407.2020.9365637.

[13] M. Charles *et al.*, 'The effect of AlN nucleation temperature on inverted pyramid defects in GaN layers grown on 200 mm silicon wafers', *J. Cryst. Growth*, vol. 464, pp. 164–167, Apr. 2017, doi: 10.1016/j.jcrysgro.2016.11.049.

[14] M. Charles, Y. Baines, R. Bouis, and A.-M. Papon, 'The Characterization and Optimization of GaN Cap Layers and SiN Cap Layers on AlGaN/GaN HEMT Structures Grown on 200 mm GaN on Silicon', *Phys. Status Solidi B*, vol. 255, no. 5, p. 1700406, May 2018, doi: 10.1002/pssb.201700406.

[15] J. He, M. Hua, Z. Zhang, and K. J. Chen, 'Performance and VTH Stability in E-Mode GaN Fully Recessed MIS-FETs and Partially Recessed MIS-HEMTs With LPCVD-SiNx/PECVD-SiNx Gate Dielectric Stack', *IEEE Trans. Electron Devices Electron Devices IEEE Trans. IEEE Trans Electron Devices*, vol. 65, no. 8, pp. 3185-3185–3191, Aug. 2018, Accessed: Apr. 08, 2020..